Monthly Notices of the ROYAL ASTRONOMICAL SOCIETY

Mon. Not. R. Astron. Soc. **416,** 205–215 (2011) doi:10.1111/j.1365-2966.2011.19022.x

Long-term spectral and timing properties of the soft gamma-ray repeater SGR 1833−0832 and detection of extended X-ray emission around the radio pulsar PSR B1830−08

P. Esposito,[1★] G. L. Israel,[2] R. Turolla,[3,4] F. Mattana,[5] A. Tiengo,[6] A. Possenti,[1] S. Zane,[4] N. Rea,[7] M. Burgay,[1] D. Götz,[8] S. Mereghetti,[6] L. Stella,[2] M. H. Wieringa,[9] J. M. Sarkissian,[9] T. Enoto,[10] P. Romano,[11] T. Sakamoto,[12] Y. E. Nakagawa,[13] K. Makishima,[13,14] K. Nakazawa,[14] H. Nishioka[14] and C. François-Martin[15]

[1]*INAF – Osservatorio Astronomico di Cagliari, località Poggio dei Pini, strada 54, I-09012 Capoterra, Italy*
[2]*INAF – Osservatorio Astronomico di Roma, via Frascati 33, I-00040 Monteporzio Catone, Italy*
[3]*Università di Padova, Dipartimento di Fisica, via F. Marzolo 8, I-35131 Padova, Italy*
[4]*Mullard Space Science Laboratory, University College London, Holmbury St Mary, Dorking, Surrey RH5 6NT*
[5]*François Arago Centre, APC (Université Paris Diderot, CNRS/IN2P3, CEA/DSM, Observatoire de Paris), 13 rue Watt, F-75205 Paris Cedex 13, France*
[6]*INAF – Istituto di Astrofisica Spaziale e Fisica Cosmica – Milano, via E. Bassini 15, I-20133 Milano, Italy*
[7]*Institut de Ciències de l'Espai (CSIC–IEEC), Campus UAB, Facultat de Ciències, Torre C5-parell, E-08193 Barcelona, Spain*
[8]*AIM (UMR 7158 CEA/DSM-CNRS-Université Paris Diderot) Irfu/Service d'Astrophysique, Saclay, F-91191 Gif-sur-Yvette Cedex, France*
[9]*Australia Telescope National Facility, CSIRO Astronomy and Space Science, PO Box 76, Epping 1710, Australia*
[10]*Kavli Institute for Particle Astrophysics & Cosmology (KIPAC), SLAC/Stanford University, PO Box 20450, MS 29, Stanford, CA 94309, USA*
[11]*INAF – Istituto di Astrofisica Spaziale e Fisica Cosmica – Palermo, via U. La Malfa 153, I-90146 Palermo, Italy*
[12]*NASA Goddard Space Flight Center, Greenbelt, MD 20771, USA*
[13]*High Energy Astrophysics Laboratory, Institute of Physical and Chemical Research (RIKEN), Wako, Saitama 351-0198, Japan*
[14]*Department of Physics, University of Tokyo, 7-3-1 Hongo, Bunkyo-ku, Tokyo 113-0033, Japan*
[15]*Université Denis Diderot – Paris 7, 4 place Jussieu, F-75252 Paris Cedex 5, France*

Accepted 2011 May 6. Received 2011 May 4; in original form 2011 April 12

ABSTRACT

SGR 1833−0832 was discovered on 2010 March 19, thanks to the *Swift* detection of a short hard X-ray burst and follow-up X-ray observations. Since then, it was repeatedly observed with *Swift*, *Rossi X-ray Timing Explorer* and *XMM–Newton*. Using these data, which span about 225 d, we studied the long-term spectral and timing characteristics of SGR 1833−0832. We found evidence for diffuse emission surrounding SGR 1833−0832, which is most likely a halo produced by the scattering of the point-source X-ray radiation by dust along the line of sight, and we show that the source X-ray spectrum is well described by an absorbed blackbody, with temperature $kT \sim 1.2$ keV and absorbing column $N_{\rm H} = (10.4 \pm 0.2) \times 10^{22}$ cm^{-2}, while different or more complex models are disfavoured. The source persistent X-ray emission remained fairly constant at $\sim 3.7 \times 10^{-12}$ erg cm^{-2} s^{-1} for the first $\sim$20 d after the onset of the bursting episode, then it faded by a factor of $\sim$40 in the subsequent $\sim$140 d, following a power-law trend with index $\alpha \simeq -0.5$. We obtained a phase-coherent timing solution with the longest baseline ($\sim$225 d) to date for this source which, besides period $P = 7.565\,4084(4)$ s and period derivative $\dot{P} = 3.5(3) \times 10^{-12}$ s s^{-1}, includes higher order period derivatives. We also report on our search of the counterpart to the soft gamma-ray repeater (SGR) at radio frequencies using the Australia Telescope Compact Array and the Parkes Radio Telescope. No evidence for radio emission was found, down to flux densities of 0.9 mJy (at 1.5 GHz) and 0.09 mJy (at 1.4 GHz) for the continuum and pulsed emissions, respectively, consistently with other observations at different epochs. Finally, the analysis of the field of PSR B1830−08

★E-mail: paoloesp@oa-cagliari.inaf.it

© 2011 The Authors
Monthly Notices of the Royal Astronomical Society © 2011 RAS

Downloaded from http://mnras.oxfordjournals.org/ at University College London on April 29, 2013

(J1833−0827), which was serendipitously imaged by the *XMM–Newton* observations, led to the discovery of the X-ray pulsar wind nebula generated by this 85-ms radio pulsar. We discuss its possible association with the unidentified TeV source HESS J1834−087.

Key words: stars: neutron – pulsars: general – X-rays: individual: PSR B1830−08 (J1833−0827) – X-rays: individual: SGR 1833−0832.

1 INTRODUCTION

Soft gamma-ray repeaters (SGRs; seven confirmed members) and anomalous X-ray pulsars (AXPs; 12 confirmed members)[1] are two classes of X-ray pulsating sources with no evidence for companion stars which share a number of properties. These include rotation periods of several seconds ($P \sim 2$–12 s), rapid spin-down ($\dot{P} \sim 10^{-11}$ s s^{-1}), large and variable X-ray luminosities (exceeding the rate of rotational energy loss), and the emission of flares and short bursts (see Woods & Thompson 2006; Mereghetti 2008 for reviews). SGRs and AXPs (note that the distinction is becoming increasingly blurred) are currently interpreted as observational manifestations of magnetars, namely neutron stars powered by their huge magnetic field (e.g. Paczynski 1992; Duncan & Thompson 1992; Thompson & Duncan 1995, 1996; Thompson, Lyutikov & Kulkarni 2002). This picture is supported by the fact that the dipole magnetic fields inferred for SGRs and AXPs from their period and period derivative[2] are above, or at the high end of, those of the radio pulsars. Surface magnetic fields in SGRs/AXPs in fact often exceed 10^{14} G, although an upper limit as low as 7.5×10^{12} G has been recently reported for SGR 0418+5729 (Rea et al. 2010).

Between periods of activity, characterized by bursts and significant variability in flux, spectrum, pulse shape and spin-down rate, magnetars go through long stretches of quiescence. The discovery of the first 'transient' AXP, XTE J1810−197 (Ibrahim et al. 2004),[3] showed that during quiescence magnetars can be faint and not dissimilar from hundreds of unidentified sources present in various X-ray catalogues (such as the *ROSAT*, *XMM–Newton* and *Chandra* ones). This suggested that a potentially large number of magnetars had not been discovered yet and may manifest themselves in the future. Thanks also to the effectiveness of the *Swift* and *Fermi* satellites in catching magnetar outbursts; five new magnetars (all of them transients) were discovered in the last few years, and several major outbursts were observed from known sources (see Rea & Esposito 2011 and references therein).

A recent addition to the magnetar family is SGR 1833−0832. It was discovered on 2010 March 19 when, at 18:34:50 UT, the *Swift* Burst Alert Telescope (BAT) triggered on a short (<1 s) hard ray burst and localized it in a region close to the Galactic plane (Barthelmy et al. 2010; Gelbord et al. 2010; Göğüş et al. 2010a). The *Swift* X-ray Telescope (XRT) started observing the BAT field one minute after the trigger and unveiled the existence of a previously unknown bright X-ray source. Given the proximity to the Galactic plane and the burst properties, the X-ray source was immediately suggested to be an SGR. The SGR nature of the source, now catalogued as SGR 1833−0832, has been confirmed shortly after by the discovery with *Swift* and *Rossi X-ray Timing Explorer* (*RXTE*) of pulsations at 7.57 s (Esposito et al. 2010a; Göğüş et al. 2010b; Palmer & Gelbord 2010). Subsequent observations also allowed the determination of the spin-down rate of SGR 1833−0832 (Esposito et al. 2010c; Göğüş et al. 2010a). Following the onset of the outburst, the source flux remained fairly constant for about 20 d (Göğüş et al. 2010a). No radio, optical or infrared counterparts have been detected (Burgay et al. 2010; Göğüş et al. 2010a; Wieringa et al. 2010).

Here we report on the spatial and long-term spectral and temporal behaviour of the persistent X-ray emission of SGR 1833−0832 using new *XMM–Newton*, *RXTE* and *Swift* observations. In Sections 2 and 3 we describe the X-ray observations used in our study and we present the results of our analysis. In Section 4 we give more details on the radio observations presented in Burgay et al. (2010) and Wieringa et al. (2010). In Section 5 we report on the analysis of the field of PSR B1830−08 (J1833−0827), which was serendipitously imaged by the *XMM–Newton* observations, and discuss its possible association with the unidentified TeV source HESS J1834−087. Discussion follows in Section 6.

2 X-RAY OBSERVATIONS

2.1 *XMM–Newton*

The three focal plane CCD cameras of the *XMM–Newton* EPIC instrument, pn (Strüder et al. 2001), MOS1 and MOS2 (Turner et al. 2001), cover the 0.1–12 keV energy range with an effective area of roughly 1400 cm^2 for the pn and 600 cm^2 for each MOS. After the discovery of SGR 1833−0832, *XMM–Newton* pointed its mirrors towards the new SGR three times (see Table 1). All observations were performed with the thick optical filter and in full frame mode,[4] except for the first one, carried out with the MOS cameras in large window mode. Moreover, *XMM–Newton* serendipitously imaged the field of SGR 1833−0832 on 2006 September 16 during an observation targeting the nearby supernova remnant G23.5–0.0 (Obs ID: 0400910101, exposure: 12.4 ks; all the detectors were in full frame mode with the medium filter).

The data were processed using version 10.0 of the *XMM–Newton* Science Analysis Software (SAS) and standard screening criteria were applied. Source events were accumulated for each camera from circular regions with a 36 arcsec radius. We selected this aperture, corresponding to ∼85 per cent of the encircled energy fraction

[1] See the McGill Pulsar Group catalogue at the web page http://www.physics.mcgill.ca/∼pulsar/magnetar/main.html.

[2] According to the usual magnetic braking formula, for a neutron star of 10 km radius and 1.4 solar masses, $B_{\rm dip} \approx 3.2 \times 10^{19}(P\dot{P})^{1/2}$ G (e.g. Lorimer & Kramer 2004).

[3] Actually, at that time another magnetar with a transient behaviour, SGR 1627−41 (Kouveliotou et al. 2003; Esposito et al. 2008), was already known, but its characteristics were not well established yet. Significant flux variability was reported also in the AXP candidate AX J1845.0−0300 (Torii et al. 1998; Vasisht et al. 2000; Tam et al. 2006).

[4] See the *XMM–Newton* User Handbook at http://xmm. esac. esa. int/ external/ xmm_user_support/documentation/index.shtml.

Downloaded from http://mnras.oxfordjournals.org/ at University College London on April 29, 2013

Table 1. Journal of the *Swift* and *XMM–Newton* observations. The time of the BAT trigger is MJD 55274.774.

Instrument	Obs. ID	Start date (MJD)	Exposure (ks)
Swift	00416485000	55274.775	29.1
Swift	00416485001	55276.177	10.8
Swift	00416485002[a]	55276.700	10.0
Swift	00416485003	55277.327	9.9
XMM–Newton	0605851901	55278.525	22.0
Swift	00416485004	55278.374	8.1
Swift	00416485005	55279.047	10.3
Swift	00416485006	55280.067	9.8
Swift	00416485007	55281.520	10.0
Swift	00416485008	55282.457	9.9
Swift	00416485009	55283.003	10.9
Swift	00416485010	55284.531	9.5
Swift	00416485011	55286.014	7.9
XMM–Newton	0605852001	55288.503	21.0
Swift	00416485012	55289.625	10.0
Swift	00416485013	55293.573	10.1
Swift	00416485014	55298.406	5.1
Swift	50041648015	55299.133	4.0
XMM–Newton	0605852101	55299.187	19.0
Swift	00416485016	55301.003	9.4
Swift	00416485017	55304.623	8.8
Swift	00416485018	55307.163	10.3
Swift	00416485019	55309.117	7.6
Swift	00416485020	55315.653	5.5
Swift	00416485021	55316.055	4.4
Swift	00416485022	55339.813	18.0
Swift	00416485023	55432.162	5.3
Swift	00416485024	55433.372	2.2
Swift	00416485025	55434.106	9.9
Swift	00416485026	55435.242	2.5

[a]This observation was carried out in windowed timing (WT) mode.

at 5 keV for a point source, in order to minimize the contamination from the diffuse emission surrounding SGR 1833−0832 (see Section 3.1). The background counts were extracted from source-free regions far from the position of the SGR. The ancillary response files and the spectral redistribution matrices for the spectral analysis were generated with the SAS tasks ARFGEN and RMFGEN, respectively.

2.2 *Swift*

The XRT (Burrows et al. 2005) onboard *Swift* uses a CCD detector sensitive to photons between 0.2 and 10 keV with an effective area of about 110 cm^2. 27 observations of SGR 1833−0832 were performed (see Table 1), starting right after its discovery, in both photon counting (PC) and windowed timing (WT) modes (see Hill et al. 2004 for more details on the XRT readout modes). The results of the first 18 *Swift* observations have already been published in Göğüş et al. (2010a), while the others are reported here for the first time.

The data were processed and filtered with standard criteria using the FTOOLS software package. We extracted the PC source events from a circle with a radius of 15 pixels (1 pixel corresponds to about 2.36 arcsec) and the WT data from a 25-pixel-wide strip. To estimate the background, we extracted PC and WT events from source-free regions distant from the position of SGR 1833−0832. For the spectral fitting, we used the latest available spectral redistribution matrix in CALDB (v011), while the ancillary response files were generated with XRTMKARF, and they account for different extraction regions, vignetting and point spread function (PSF) corrections.

2.3 *RXTE*

The Proportional Counter Array (PCA; Jahoda et al. 1996) onboard *RXTE* consists of an array of five collimated xenon/methane multi-anode Proportional Counter Units (PCUs) operating in the 2–60 keV energy range, with a total effective area of approximately 6500 cm^2 and a full width at half-maximum field of view (FOV) of about 1°. The 80 *RXTE*/PCA pointed observations of SGR 1833−0832 (Obs. ID: 95048) reported here span from 2010 March 19 to 2010 December 4. The exposures range from 1 to 20 ks, for a total of about 466.4 ks. The results of the first 31 *RXTE* observations have already been published in Göğüş et al. (2010a), while the analysis of the others is reported here for the first time.

The raw data were reduced using the FTOOLS package. Given the non-imaging nature and wide FOV of the PCA instrument and the relatively low flux of SGR 1833−0832, the *RXTE* data were used only to study the timing properties of the source. We thus restricted our analysis to the data in Good Xenon mode, with a time resolution of 1 μs and 256 energy bins. They were extracted in the 2–10 keV energy range from all active PCUs (in a given observation) and all layers, and binned into light curves of 10-ms resolution.

3 X-RAY DATA ANALYSIS AND RESULTS

We inspected all observations for the presence of bursts by a careful examination of the light curves binned with different time resolutions. A few were found (besides those reported in Göğüş et al. 2010a, we found another short and weak burst in the *RXTE* data of 2010 May 18). In the analyses that follow, we removed the bursts from the event lists by applying intensity filters. *Swift* and *RXTE* data from a few contiguous observations carried out with the same instrumental setup were combined in order to achieve better statistics and higher signal-to-noise ratio. For the timing analysis, the data were corrected to the barycentre of the Solar system using the *Chandra*/United Kingdom Infrared Telescope position reported in Göğüş et al. (2010a).

3.1 Spatial analysis

As can be seen in Fig. 1, some diffuse emission around SGR 1833−0832 was detected during the three *XMM–Newton* observations, mainly in the 3–6 keV energy band. Considering the large absorption derived from the X-ray spectrum, this is likely a halo produced by the scattering of the point-source X-ray radiation by dust along the line of sight (Overbeck 1965; Rivera-Ingraham & van Kerkwijk 2010; Tiengo et al. 2010).

By analysing the spectrum from different annular regions, we have found that, as expected from a dust halo, the diffuse X-ray emission is significantly softer than the point source. Moreover, the *XMM–Newton* observation of the SGR 1833−0832 field performed in 2006, where neither point-like nor diffuse emission was detected at the SGR position (see Section 3.4), favours the dust halo hypothesis with respect to steady diffuse emission, as expected, for example, in a supernova remnant. However, the data quality of the outburst observations is not good enough to detect significant variability in the extended emission at the level expected for a dust-scattering halo.

© 2011 The Authors, MNRAS **416,** 205–215
Monthly Notices of the Royal Astronomical Society © 2011 RAS

Downloaded from http://mnras.oxfordjournals.org/ at University College London on April 29, 2013

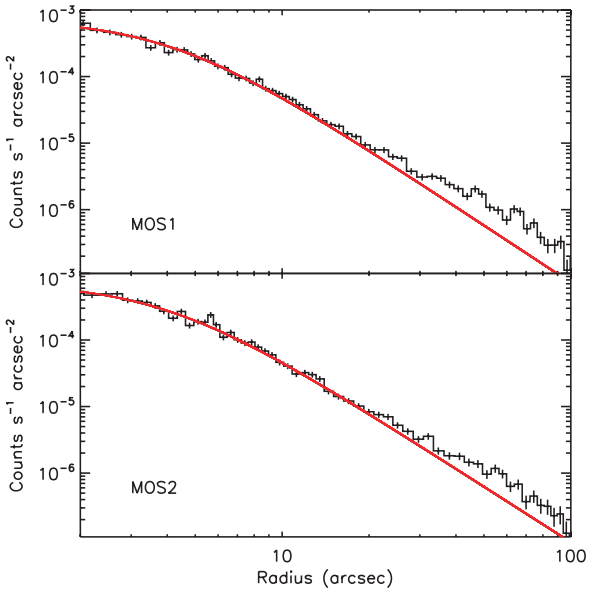

Figure 1. Surface brightness radial profiles of the background-subtracted X-ray emission of SGR 1833−0832 from the *XMM–Newton* MOS1 and MOS2 cameras (3–6 keV data from the three observations combined). The red solid line shows for each camera the best-fitting PSF (Ghizzardi 2001). The radial profiles show clear evidence for extended emission starting from ∼35 arcsec.

3.2 Spectral analysis

For the spectroscopy (performed with the XSPEC 12.6 fitting package; Arnaud 1996) we concentrate first on the *XMM–Newton* spectra which, owing to the EPIC instrument high throughput and long observing time, are those with the best statistical quality. We fit the spectra from the three observations simultaneously with the hydrogen column density tied between all data sets. Photons having energies below 2 keV and above 10 keV were ignored, owing to the very few counts from SGR 1833−0832. This resulted in about 6100 ± 80, 5800 ± 90 and 4000 ± 70 net EPIC-pn counts in the three observations in chronological order. The abundances used are those of Anders & Grevesse (1989) and photoelectric absorption cross-sections are from Balucinska-Church & McCammon (1992).

Using the first 12 *Swift*/XRT observations in PC mode, Göğüş et al. (2010a) could not discriminate between a power law and a blackbody as the model that better describes the spectrum of the SGR persistent emission. A fit of the *XMM–Newton* pn and MOS data with an absorbed power law yields a relatively high χ^2 value [$\chi^2_\nu = 1.21$ for 673 degrees of freedom (d.o.f.)] and structured residuals, while a better fit ($\chi^2_\nu = 1.05$ for 673 d.o.f.) is obtained using a blackbody model (corrected for the absorption). No additional spectral components are statistically required. The results of this simultaneous modelling are presented in Table 2 (the values of the spectral parameters were not significantly different when each observation was fitted separately). The best-fitting hydrogen column density is $(10.4 \pm 0.2) \times 10^{22}$ cm^{-2} (here and in the following uncertainties are at 1σ confidence level, unless otherwise noted) and the blackbody temperature is consistent within the errors with being constant at $kT \simeq 1.2$ keV, while the observed flux slightly (but significantly, see Table 2) decreased from $F \simeq 3.9 \times 10^{-12}$ to 3.1×10^{-12} erg cm^{-2} s^{-1} (in the 2–10 keV band) during the ∼20 d that separate the first and last *XMM–Newton* pointings. Assuming an arbitrary distance of 10 kpc, the corresponding *XMM–Newton* maximum and minimum luminosities are $\sim 9 \times 10^{34}$ and $\sim 7 \times 10^{34}$ erg s^{-1} (Table 2). For each *XMM–Newton* observation, we performed phase-resolved spectroscopy by extracting the spectra for different selections of phase intervals. No significant variations with phase were detected, all the spectra being consistent with the model and parameters of the phase-averaged spectrum, simply rescaled in normalization.

Most magnetars, especially when in outburst, exhibit more complex spectra, usually fitted by the superposition of two/three blackbodies or a blackbody and a high-energy power law (e.g. Mereghetti et al. 2005; Israel et al. 2007a; Bernardini et al. 2009; Enoto et al. 2009; Esposito et al. 2009; Rea et al. 2009; Bernardini et al. 2011). The spectrum of SGR 1833−0832 is reminiscent of that reported by Esposito et al. (2010b) for SGR 0418+5729 during its 2009 outburst. However, at the time of the analysis reported in Esposito et al. (2010b), only low-counts-statistics *Swift* and *RXTE* spectra were available for SGR 0418+5729. Higher quality *XMM–Newton* data, now public, clearly show that a more complex model is required for the emission of SGR 0418+5729.[5]

In order to achieve better statistics and higher signal-to-noise ratio, we merged the data from the first two *XMM–Newton* observations (since there is no evidence for variations in the flux and spectrum of the source between them) and accumulated a combined spectrum which is presented in Fig. 2. Again, the single-blackbody model provides an excellent fit ($\chi^2_\nu = 1.00$ for 352 d.o.f.), and no additional components are required. By including in the model a power-law component with photon index fixed to 3 (see e.g. Rea et al. 2009), we can set 3σ upper limits of ≈25 and 30 per cent on the contribution of this component to the total observed and unabsorbed fluxes, respectively. This shows that the relatively low flux and high absorption of SGR 1833−0832 make even our deep *XMM–Newton* observations not very sensitive to the presence of a second spectral component in this SGR. We repeated the phase-resolved spectral analysis on the combined data set. Once more, we see no evidence of spectral shape evolution with the rotational phase; in particular, no variation larger than the 1σ error ($k\delta T \simeq 0.02$ keV) was found in the blackbody temperatures at different phases.

To obtain flux measurements over the outburst, the *Swift*/XRT data were fitted in the same way as the *XMM–Newton* ones, simultaneously and with all parameters left free to vary, except for the absorption column density, that this time was fixed at the value measured with *XMM–Newton*. This resulted in an acceptable fit ($\chi^2_\nu = 1.01$ for 602 d.o.f.) with spectral parameters similar to those reported in Table 2 (see Fig. 3). We plot the resulting long-term light curve in the top panel of Fig. 3.

Although the available data do not allow us to perform an accurate modelling of the decay shape because of the relatively high uncertainties on the fluxes and moderate time-span, we observe that similarly good fits can be obtained with either an exponential function or a broken power law model. For an exponential function of the form $F(t) = A\exp(-t/\tau)$, the best-fitting values ($\chi^2_\nu = 0.84$

[5] We have analysed an *XMM–Newton* observation of SGR 0418+5729 performed on 2009 August 12–13, about 68 d after the outburst onset (Obs. ID 0610000601, exposure 67.2 ks). The data are well described by a power law plus blackbody model ($\chi^2_\nu = 1.1$ for 231 d.o.f.) with the following spectral parameters: $N_{\rm H} = (6.4 \pm 0.3) \times 10^{21}$ cm^{-2}, photon index $\Gamma = 2.6^{+0.2}_{-0.1}$, blackbody temperature $kT = 0.93 \pm 0.01$ keV, and 0.5–10 keV absorbed flux $(7.0 \pm 0.2) \times 10^{-12}$ erg cm^{-2} s^{-1}. A double blackbody gave a poorer fit ($\chi^2_\nu = 1.2$ for 231 d.o.f.), whereas both blackbody and power-law models yield statistically unacceptable fits ($\chi^2_\nu \gg 2$).

Downloaded from http://mnras.oxfordjournals.org/ at University College London on April 29, 2013

Table 2. Spectral fit of the *XMM–Newton* data with the blackbody model ($\chi^2_\nu = 1.05$ for 673 d.o.f.). Errors are at a 1σ confidence level for a single parameter of interest. The measured $N_{\rm H}$ value is $(10.4 \pm 0.2) \times 10^{22}$ cm^{-2}.

Obs.ID	kT (keV)	Radius[a] (km)	Absorbed flux[b] (10^{-12} erg cm^{-2} s^{-1})	Luminosity[c] (10^{34} erg s^{-1})
060 585 1901	1.20 ± 0.01	0.62 ± 0.02	3.9 ± 0.1	$8.9^{+0.2}_{-0.1}$
060 585 2001	$1.18^{+0.02}_{-0.01}$	0.62 ± 0.02	3.6 ± 0.1	8.4 ± 0.1
060 585 2101	$1.20^{+0.02}_{-0.01}$	0.55 ± 0.02	3.1 ± 0.1	7.2 ± 0.1

[a]The blackbody radius is calculated at infinity and for an arbitrary distance of 10 kpc.
[b]In the 2–10 keV energy range.
[c]In the 2–10 keV energy range and for an arbitrary distance of 10 kpc.

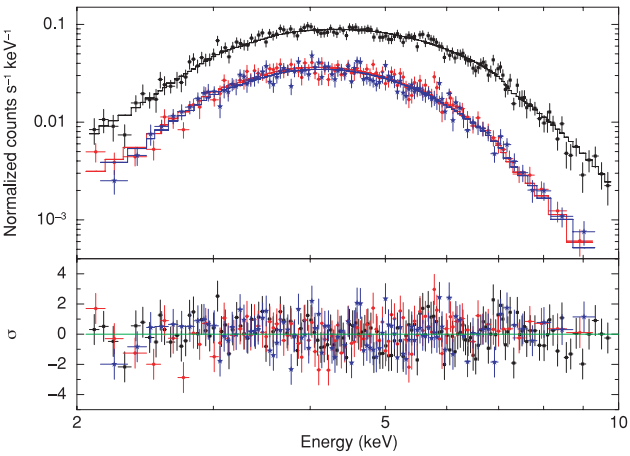

Figure 2. Fit of the spectrum obtained from the first two *XMM–Newton* observations (see Section 3.2) with the single-blackbody model. Black squares, red circles and blue stars represent the pn, MOS1 and MOS2 data, respectively. Bottom panel: the residuals of the fit (in units of standard deviations).

for 23 d.o.f.) are $A = (3.92 \pm 0.05) \times 10^{-12}$ erg cm^{-2} s^{-1} and $\tau = (108 \pm 9)$ d.[6] Adopting a broken power law ($\chi^2_\nu = 0.73$ for 22 d.o.f.), the break occurs at (20 ± 3) d, when the index changes from $\alpha_1 = -0.01 \pm 0.02$ to $\alpha_2 = -0.54 \pm 0.09$; the flux at the break time is $(3.7 \pm 0.2) \times 10^{-12}$ erg cm^{-2} s^{-1}. In both cases, we assumed as $t = 0$ the time of the *Swift*/BAT trigger. From the broken power law fit in particular, it is apparent that the source flux is consistent with a constant value for the first ∼20 d. The two models considered are plotted in Fig. 3.

3.3 Timing analysis

In Esposito et al. (2010a), we reported on our search for periodicities made on the first *Swift*/XRT observation (00416485000) by calculating a fast Fourier transform power spectrum. A very prominent peak occurs in the spectrum of that observation at 7.5653(4) s (the quoted uncertainty indicates the Fourier period resolution). Pulsations were clearly detected also in all the other *Swift* and *XMM–Newton* data sets, and in the *RXTE* ones up to 2010 October 30 (MJD 55499), when presumably the flux became too low for the PCA sensitivity.

In order to obtain a refined ephemeris for the longest possible baseline, we studied the pulse phase evolution in these observations

[6] An additional component F_0 representing the base flux level $[F(t) = F_0 + A\exp(-t/\tau)]$ is not required. Including it anyway in the fit ($\chi^2_\nu \simeq 0.83$ for 22 d.o.f.), we find $F_0 = (5 \pm 4) \times 10^{-13}$ erg cm^{-2} s^{-1}.

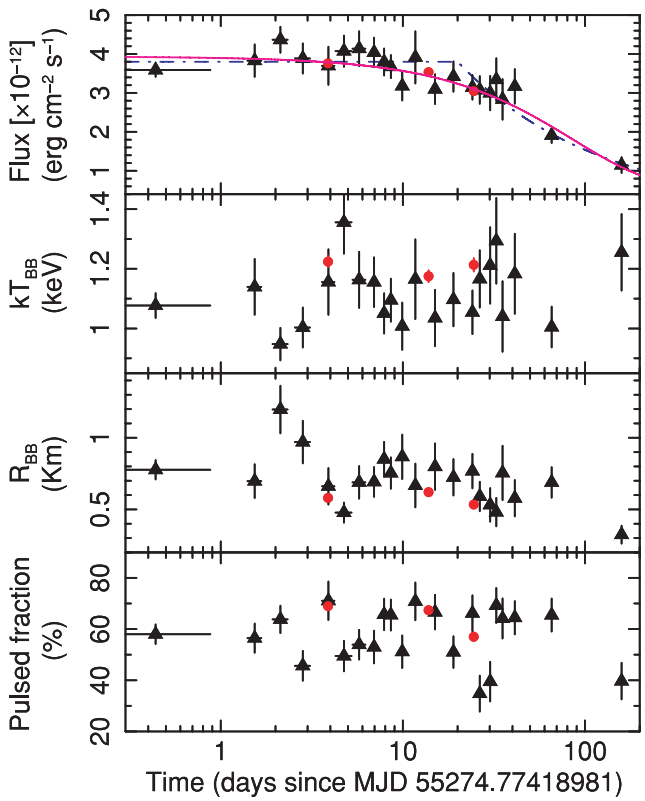

Figure 3. Time evolution of the characteristic parameters of SGR 1833−0832 inferred from the spectral analysis (single-blackbody model) of the *Swift* (black triangles) and *XMM–Newton* (red circles) data. The different panels show (from top to bottom) the (absorbed) flux in the 2–10 keV energy range (two possible models describing the decay are also plotted: an exponential function with the solid magenta line and a broken power law with the dot–dashed blue line; see Section 3.2), the blackbody temperature and radius (evaluated at infinity and assuming an arbitrary distance of 10 kpc), and the pulsed fraction. We assumed as $t = 0$ the time of the *Swift*/BAT trigger.

by means of an iterative phase-fitting technique (see e.g. Dall'Osso et al. 2003). The fits were carried out in the range 2–10 keV with a χ^2 minimization approach using MINUIT (James & Roos 1975).

Throughout the period covered by useful observations (∼225 d) the relative phases and amplitudes were such that the phase evolution of the signal could be followed unambiguously. A second-order polynomial, as employed in the recent analysis by Göğüş et al. (2010a) over the first ∼47 d, provides an unacceptable fit to the data, with $\chi^2_\nu = 9.06$ for 86 d.o.f. We tried higher order polynomials until the addition of a further (higher order) term was not

Downloaded from http://mnras.oxfordjournals.org/ at University College London on April 29, 2013

Table 3. Spin ephemeris of SGR 1833−0832 obtained using the combined *RXTE*, *Swift* and *XMM–Newton* observations. We also give for convenience the corresponding period P and period derivative $\dot{P}$, as well as the derived characteristic age $\tau_c = P/(2\dot{P})$, dipolar magnetic field $B \approx (3c^3 I P \dot{P}/8\pi^2 R^6)^{1/2}$, and rotational energy loss $\dot{E} = 4\pi^2 I \dot{P} P^{-3}$ (here we took $R = 10$ km and $I = 10^{45}$ g cm^2 for the star radius and moment of inertia, respectively).

Parameter	Value
Range (MJD)	55274.775–55499.170
Epoch (MJD)	55274.0
ν (Hz)	0.132 180 571(7)
$\dot{\nu}$ (Hz s^{-1})	$-6.0(5) \times 10^{-14}$
$\ddot{\nu}$ (Hz s^{-2})	$-1.3(2) \times 10^{-20}$
$\dddot{\nu}$ (Hz s^{-3})	$9(2) \times 10^{-28}$
χ^2/d.o.f.	89.47/84
P (s)	7.565 408 4(4)
$\dot{P}$ (s s^{-1})	$3.5(3) \times 10^{-12}$
τ_c (kyr)	35
B (G)	1.6×10^{14}
$\dot{E}$ (erg s^{-1})	3.2×10^{32}

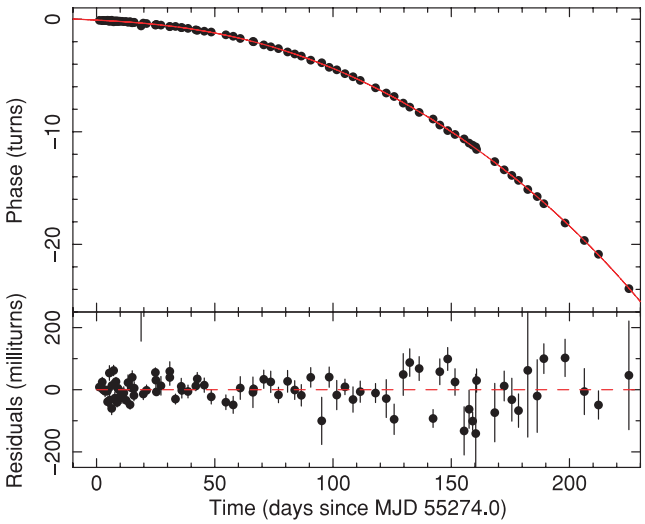

Figure 4. Top panel: *Swift*, *XMM–Newton* and *RXTE* pulse phase evolution with time with respect to the period measured during the first *Swift* observation. The solid red line represents the best-fitting fourth-order polynomial solution. Bottom panel: time residuals with respect to timing solution.

statistically significant at more than 3σ with respect to the null hypothesis (as evaluated by the Fisher test). The outcome of this process was a fourth-order polynomial (the improvement obtained in the fit with a fifth-order polynomial has a statistical significance of only 2.6σ), which we used to fit the phase shifts. The resulting phase-coherent solution is given in Table 3 and plotted in Fig. 4; the best fit ($\chi^2_\nu = 1.07$ for 84 d.o.f.) gives $\nu = 0.132\,180\,571(7)$ Hz and $\dot{\nu} = -6.0(5) \times 10^{-14}$ Hz s^{-1}, assuming MJD 55274.0 as reference epoch. We have checked that the positional uncertainty (0.3 arcsec; Göğüş et al. 2010a) does not significantly affect the rotational parameters resulting from our analysis.

In Fig. 5 we show the three *XMM–Newton* light curves obtained folding the high time resolution (nominal frame time of 73.4 ms) EPIC-pn data at our phase-coherent ephemeris. The pulse profile is sinusoidal and the pulsed fraction, which we define as the semi-amplitude of sinusoidal modulation divided by the mean

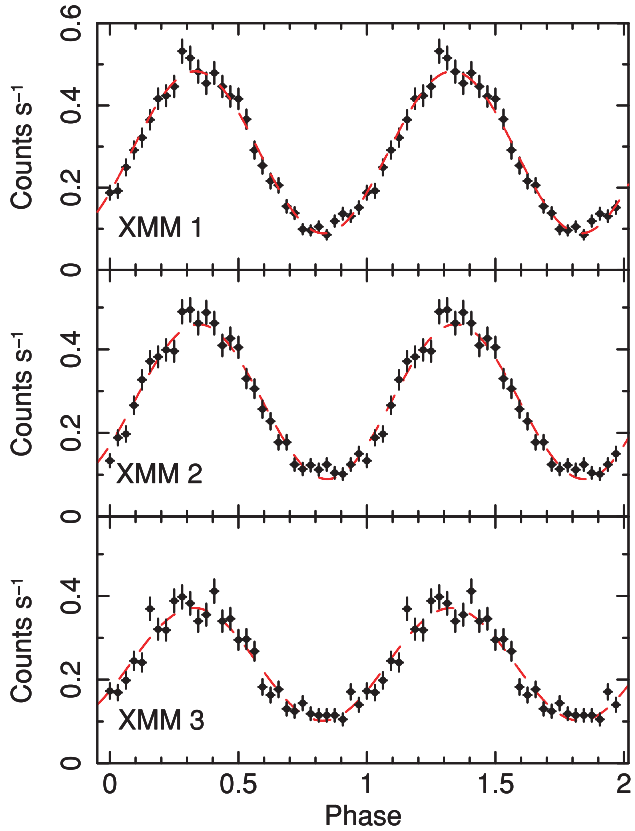

Figure 5. Background-subtracted *XMM–Newton* epoch-folded pulse profiles (32-bin, EPIC-pn). The sinusoidal fit to the data is superimposed in red (the χ^2_ν values are 0.9, 1.0 and 1.2 for 29 d.o.f., for the three observations in order).

source count rate, was consistent through the first two observations [(69.0 ± 1.4) and (67.4 ± 1.5) per cent, respectively], while it decreased to (57.0 ± 1.7) per cent in the third one. We have investigated the morphology of the pulse phase distribution as a function of energy by comparing the *XMM–Newton* pulse profiles in different energy bands. The measured pulsed fractions in the three observations are (66 ± 2), (64 ± 2) and (56 ± 2) per cent in the soft (2–5 keV) energy band, and (75 ± 2), (71 ± 2) and (59 ± 3) per cent in the hard (5–10 keV) band. Apart from this marginal indication for an increasing trend of the pulsed fraction with energy, no significant pulse shape variations (such as phase shifts of the maxima) were found as a function of energy by cross-correlating or comparing through a two-sided Kolmogorov–Smirnov test the soft- and hard-folded profiles.

The 2–10 keV pulsed fractions measured in the individual observations obtained with *XMM–Newton* and *Swift* are shown in the bottom panel of Fig. 3 (we did not consider the *RXTE* data as the non-imaging PCA instrument does not ensure reliable background subtraction). A constant fit of the pulsed fraction values derived with XRT[7] (and shown in Fig. 3) does not adequately describe the data ($\chi^2_\nu = 4.52$ for 24 d.o.f.); however, no particular trend is apparent in the pulsed fraction evolution and the simple functions we tried do not yield significantly better fits.

[7] We did not attempt to fit simultaneously the *XMM–Newton* and *Swift* data in order to avoid possible effects due to the different responses and energy dependence of the effective areas of the of the EPIC and XRT detectors.

Downloaded from http://mnras.oxfordjournals.org/ at University College London on April 29, 2013

3.4 Archival searches

No X-ray source was detected at the *Chandra* position of SGR 1833−0832 (Göğüş et al. 2010a) in the *XMM–Newton* observation performed in 2006. In a 20-arcsec circle centred at the SGR coordinates we detected in the 2–10 keV energy band 24 EPIC/pn counts (we did not use the MOS data since the source position fell near CCD gaps in both cameras). The net exposure time was 9.2 ks. Considering the expected background counts (estimated from large surrounding source-free regions) and assuming Poissonian fluctuations, we set a 3σ upper limit on the 2–10 keV count rate of SGR 1833−0832 of 2.3×10^{-3} counts s^{-1}. Assuming a blackbody spectrum with $kT = 1.2$ keV and an absorption of $N_{\rm H} = 10.4 \times 10^{22}$ cm^{-2}, this translates into an upper limit on the 2–10 keV observed flux of $\sim 4 \times 10^{-14}$ and of $\sim 8 \times 10^{-14}$ erg cm^{-2} s^{-1} on the 2–10 keV unabsorbed flux. If instead we assume a much softer blackbody spectrum with $kT = 0.3$ keV, as it might be expected from a magnetar in quiescence (e.g. Lamb et al. 2002; Gotthelf et al. 2004; Bernardini et al. 2009), the following upper limits are derived (2–10 keV band): $\sim 2 \times 10^{-14}$ erg cm^{-2} s^{-1} on the observed and $\sim 2 \times 10^{-13}$ erg cm^{-2} s^{-1} on the unabsorbed flux.

More recently, on 2009 February 13, the field of SGR 1833−0832 was serendipitously imaged for 8 ks by the *Chandra*/ACIS-S (see also Misanovic, Kargaltsev & Pavlov 2011). The SGR was not detected and Göğüş et al. (2010a) derived a 2σ upper limit on the absorbed flux of 3.4×10^{-13} erg cm^{-2} s^{-1}, assuming a power-law model with $\Gamma \sim 3$ and $N_{\rm H} \sim 14 \times 10^{22}$ cm^{-2} (Gelbord & Vetere 2010).

4 RADIO OBSERVATIONS

4.1 ATCA

We observed the *Swift*/XRT position of SGR 1833−0832 at 20 cm twice, on 2010 March 22 (UT time 21:40–22:20) and March 23 (UT time 00:17–01:32), with a total on-source integration time of 105 min. The observing band was 1.1–1.9 GHz, split in 1 MHz channels and with a central frequency of 1.52 GHz; however, several channels, affected by radio frequency interferences, were excised from the spectrum. The array was in the hybrid configuration H168 (maximum baseline ∼4.5 km).[8]

Given the location of the source in the Galactic plane, images including the short baselines were too confused by the emission of extended sources to yield useful limits. Continuum images combining all usable frequency channels were then made considering only the long baselines, i.e. those including the antenna CA06. These images were still somewhat confused by other sources in the field and the rms noise near the field centre was twice that outside the $\sim 11 \times 80$ arcsec^2 wide beam. In particular, the local rms at the SGR position turned out to be 0.3 mJy, whence the 3σ flux density limit for an unresolved continuum radio emission from SGR 1833−0832 is 0.9 mJy.

4.2 Parkes

The source was observed on 2010 March 25 (MJD 55279.954) for 90 min at a centre frequency of 1374 MHz with the central beam of the Parkes 20 cm multibeam (MB) receiver (Staveley-Smith et al. 1996). The total 288 MHz bandwidth was split into 96 channels, each 3 MHz wide, and the time series was 1 bit sampled every 1 ms. Data have been searched for periodicities around the value obtained from the X-ray observations over a wide range of dispersion measure values (DM < 6000 pc cm^{-3}, given the very high $N_{\rm H}$ value derived from X-ray observations). A search for single dedispersed pulses was also carried out.

No radio pulsation with a period matching (within ±2.5 ms) the X-ray period, nor half of it, has been found. The single-pulse search only revealed the presence of a bright known pulsar in the beam (the 85-ms J1833−0827/B1830−08, at DM 411 pc cm^{-3}; see Section 5). The upper limit on the pulsed flux density at 20 cm wavelength is of 0.09 mJy for a duty cycle of 10 per cent, calculated for the maximum DM investigated and assuming a minimum signal-to-noise ratio of 9. The latter relatively high value for the adopted minimum signal-to-noise ratio is due to the presence of strong radio interferences at ∼7.5 s, which affect the signal folded at the SGR period.

5 X-RAY EMISSION AROUND PSR B1830−08

Inspection of the *XMM–Newton* EPIC images reveals an excess of X-ray emission north of SGR 1833−0832, encompassing the position of the middle-aged radio pulsar PSR B1830−08 (spin-down age $\tau_{\rm c} \sim 150$ kyr; Taylor, Manchester & Lyne 1993).

PSR B1830−08 is located outside, and possibly associated to, the asymmetric shell-type supernova remnant W41 (G23.3–0.3) despite an angular separation of 24 arcmin to the centre of the remnant (Kassim 1992; Gaensler & Johnston 1995). Its distance estimated through the dispersion measure (DM = 411 pc cm^3) and the NE2001 model of the Galactic electron density distribution by Cordes & Lazio (2002) is 4.6 kpc. PSR B1830−08 might also be linked to the unidentified TeV source HESS J1834−087 lying inside W41 (Aharonian et al. 2006; Albert et al. 2006). In this case, the extended TeV source would be a relic pulsar wind nebula (PWN) generated by electrons ejected by PSR B1830−08 at its birth place and up-scattering the surrounding low-energy photons (e.g. Bartko & Bednarek 2008). However, different explanations have been suggested: the TeV emission of HESS J1834−087 could result from the π^0 decay of shock-accelerated hadrons interacting with a giant molecular cloud along the line of sight (Tian et al. 2007) or from the inverse Compton radiation of electrons in a different PWN recently discovered near the centre of W41 (Mukherjee, Gotthelf & Halpern 2009; Misanovic et al. 2011). The detection of a large-scale X-ray nebula trailing the pulsar in the direction of the supernova remnant and of the TeV source would support the association between PSR B1830−08 and HESS J1834−087.

We refined the imaging analysis by considering only EPIC-MOS data from the observations 0605852001 and 0605852101, whereas PSR B1830−08 was located in the unread regions of the MOS detectors operating in Large Window mode during observation 0605851901. The EPIC-pn data of the three observations were not used either, because of a higher level of residual soft proton contamination indicated by the ratio of the surface brightness inside the FOV to the one outside the FOV (De Luca & Molendi 2004). We selected only 1- and 2-pixel events with the default flag mask.

We built background maps using the Filter Wheel Closed (FWC) event lists provided by the *XMM–Newton* background working group.[9] As the profile of the FWC maps changed since the launch

[8] See http://www.narrabri.atnf.csiro.au/observing/configs.html for more details.

[9] See http://xmm.vilspa.esa.es/external/xmm_sw_cal/background/index.shtml.

© 2011 The Authors, MNRAS **416,** 205–215
Monthly Notices of the Royal Astronomical Society © 2011 RAS

Downloaded from http://mnras.oxfordjournals.org/ at University College London on April 29, 2013

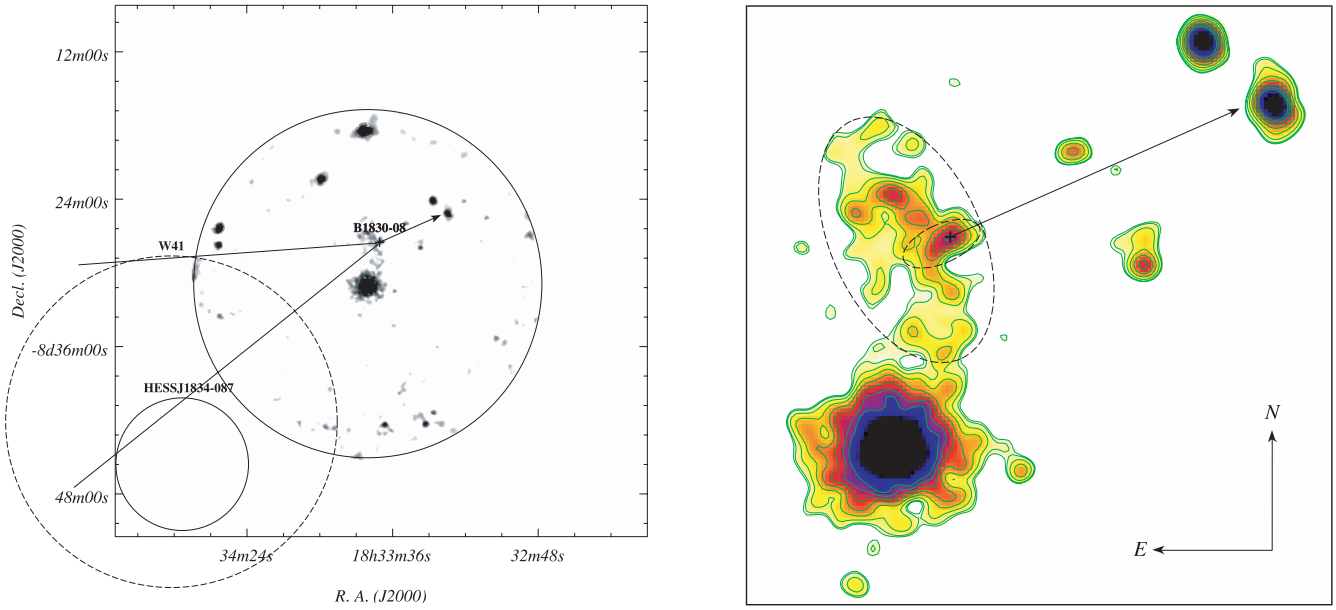

Figure 6. Left: *XMM–Newton* EPIC-MOS mosaicked image. The image is background subtracted, exposure corrected and adaptively smoothed; the intensity scale has been chosen to highlight the faint diffuse emission around PSR B1830−08. The brightest source in the centre is SGR 1833−0832. The pulsar position is marked with a cross. The arrow indicates the pulsar's measured direction of motion, the length of the arrow corresponding to the distance travelled by the pulsar over 10 kyr. The two solid lines from the pulsar position to east indicate the extrapolation of the pulsar proper motion backwards over the last 50 kyr accounting for the measured uncertainties. The large solid circle encloses the EPIC field of view. The extensions of the supernova remnant W41 (dashed circle; Kassim 1992) and of HESS J1834−087 (1σ, small solid circle; Aharonian et al. 2006) are also shown. Right: zoom-in of the EPIC-MOS mosaicked image shown in the left-hand panel. The contours are uniformly spaced. The inner and outer dashed ellipses outline the 'compact' and 'halo' emissions, respectively. The length of the compass' arms is 2 arcmin.

of the mission, we filtered only the events collected after 2007 January to produce a more accurate template of the particle-induced background. The background maps were rescaled in narrow energy bands according to the counts in the non-vignetted MOS corners. Finally, the images were mosaicked, background subtracted, exposure corrected and adaptively smoothed to achieve a signal-to-noise ratio of 6.

Diffuse emission around PSR B1830−08 is apparent in the 2–10 keV band mosaic, extending ∼2 arcmin north-east and south of the pulsar (Fig. 6, left-hand panel). A closer inspection shows a compact structure at the pulsar position embedded in a halo of lower surface brightness (Fig. 6, right-hand panel). The compact structure is ∼1 arcmin elongated towards south-east, whereas the halo is mostly extending in the perpendicular direction. The bulk of the halo emission lies closer to PSR B1830−08, while the the south-western tip is apparently connected with SGR 1833−0832; this is most likely due to the smoothing procedure. Both the halo and the compact structures are hardly visible in the soft band (0.5–2 keV), suggesting an absorbed non-thermal emission. This is confirmed by the spectral analysis.

We produced the spectra also including the three EPIC-pn data sets. The source counts were extracted from the mutually exclusive elliptical regions shown in Fig. 6 (right-hand panel). The background counts were estimated from 60-arcsec apertures placed on the same CCD of each camera, and at the same distance to the read-out node as the source for the EPIC-pn. For each EPIC camera, we merged the individual spectra from the different observations into a single spectrum and combined the response matrices. The compact and halo regions contained 560 ± 30 and 2800 ± 160 background-subtracted counts, respectively, corresponding to an average surface

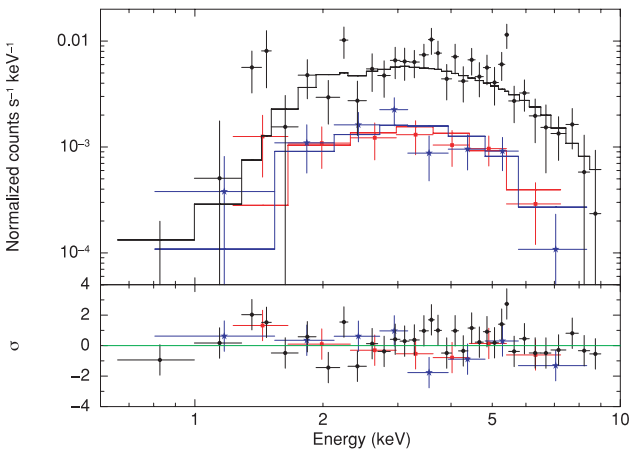

Figure 7. EPIC MOS1 (red circles), MOS2 (blue stars) and pn (black squares) spectra of the compact structure around PSR B1830−08 (inner ellipse in Fig. 6, right) fit to the model described in the text. The lower panel shows residuals from the best fit in units of 1σ.

brightness of 0.2 and 0.085 counts arcsec^{-2}. The spectra were re-binned with a minimum of 20 counts per spectral channel for the compact emission and 50 for the halo.

The EPIC pn and MOS spectra of the compact structure (Fig. 7) are well fitted by an absorbed power-law model, yielding photon index $\Gamma = 1.9^{+0.7}_{-0.6}$, unabsorbed 2–10 keV flux $F_{(2-10\,\mathrm{keV})} = (1.6^{+0.4}_{-0.2}) \times 10^{-13}$ erg cm^{-2} s^{-1}, and hydrogen-equivalent column density $N_{\mathrm{H}} = (4 \pm 2) \times 10^{22}$ cm^{-2} (reduced $\chi^2 = 1.0$ for 46 d.o.f.). The halo spectra are also well fitted by an absorbed power-law model with

Downloaded from http://mnras.oxfordjournals.org/ at University College London on April 29, 2013

$\Gamma = 1.7^{+0.5}_{-0.4}$, unabsorbed 2–10 keV flux $F_{(2-10\,\mathrm{keV})} = (5.9^{+0.7}_{-0.6}) \times 10^{-13}$ erg cm^{-2} s^{-1} and $N_{\mathrm{H}} = (2.9^{+1.3}_{-0.9}) \times 10^{22}$ cm^{-2} (reduced $\chi^2 = 1.1$ for 153 d.o.f.). By fitting simultaneously the compact and halo spectra with the same column density, we found $N_{\mathrm{H}} = (3.4^{+1.1}_{-0.9}) \times 10^{22}$ cm^{-2}, slightly higher than the neutral hydrogen column density from radio observations $\sim 2 \times 10^{22}$ cm^{-2} (Dickey & Lockman 1990), which might indicate additional absorbing material along the line of sight.

The hard diffuse emission around PSR B1830−08 is suggestive of a PWN. With a spin-down power of $\dot{E} = 5.8 \times 10^{35}$ erg s^{-1}, PSR B1830−08 is energetic enough to produce a synchrotron nebula detectable in X-rays for a broad range of distances. For an assumed distance of 4.6 kpc, the measured fluxes imply a luminosity in the 2–10 keV energy range of $\sim 4 \times 10^{32}$ erg s^{-1} for the compact structure and of $\sim 1.5 \times 10^{33}$ erg s^{-1} for the halo. This corresponds to a conversion efficiency $L_{\mathrm{X}}/\dot{E}$ of 7×10^{-4} and 3×10^{-3}, within the observed range of pulsar/PWN systems (Possenti et al. 2002; Kargaltsev & Pavlov 2008).

The inner compact structure looks one sided, and its brightness peak is coincident with the pulsar position. Such a morphology is reminiscent of a bow-shock PWN, in which the wind of a supersonically moving pulsar is confined by the ram pressure of the surrounding medium (see Gaensler & Slane 2006, for a review). This phase occurs once the pulsar escapes its remnant, several 10 000 years after the supernova event, which is compatible with the age of PSR B1830−08. Furthermore, the proper motion of PSR B1830−08 (33 ± 5 mas yr^{-1}, corresponding to a linear velocity of $730 d_{4.6}$ km s^{-1}; Hobbs et al. 2004) lies in the high-velocity end of the pulsar population and it is most likely supersonic. The compact emission seems to be aligned with the pulsar proper motion (Fig. 6, right), the brightness profile declining gradually from the pulsar position to south-east and sharply to north-west.

The location opposite to the direction of the pulsar motion, the hard extended emission and the column density suggest that the halo is also linked to PSR B1830−08. However, its morphology is different from observed (e.g. the 'Mouse' G359.23–0.82; Gaensler et al. 2004) and simulated (e.g. Bucciantini, Amato & Del Zanna 2005) bow-shock PWNe, in which the emission is tightly confined along the proper motion direction. The halo forms instead a broad diffuse region behind the pulsar, almost perpendicular to the proper motion direction.

6 DISCUSSION

6.1 SGR 1833−0832

In this work, we presented a new timing solution for SGR 1833−0832 based on a phase-coherent analysis of *XMM–Newton*, *Swift* and *RXTE* data and valid in the range from MJD 55274.775 to 55499.170. Under the standard assumption that the neutron star slows down because of magnetic braking, it implies a characteristic age $\tau_{\mathrm{c}} \simeq 35$ kyr, a dipolar magnetic field $B \approx 1.6 \times 10^{14}$ G and a rotational energy loss rate $\dot{E} \simeq 3.2 \times 10^{32}$ erg s^{-1} (see Table 3).

The modelling of the phase shifts required a fourth-order polynomial which in general is an indication for timing noise ('polynomial whitening'). However, it is worth noting that the second derivative we measured is unlikely to be related to a random change of the pulse profiles, which is expected to introduce only a random distribution of the phase residuals, rather than a cubic term. Recent studies on a sample of 366 radio pulsars showed that cubic terms in the phase residuals are actually possible, but smaller by several orders of magnitudes than those detected in SGR 1833−0832[10] and recorded on time-scales longer (years) than those we are sampling in our data set (Hobbs et al. 2010). We also note that the (long-term) timing noise of young radio pulsars (age $<10^5$ yr) can be better understood as resulting from the recovery from previous glitch events (Hobbs et al. 2010), making it unlikely that the frequency second derivative is actually due to random noise.

A possibility is therefore that the higher order frequency derivatives we observed are manifestations of a glitch recovery. In the AXP 1RXS J1708−4009, for instance, negative second frequency derivatives in the $-(0.01\text{–}1.3) \times 10^{-20}$ Hz s^{-2} range have been detected just after glitches (Israel et al. 2007b; Dib, Kaspi & Gavriil 2008). We found no evidence for glitches in the time spanned by our observations, but this does not exclude the possibility that such events occurred before the first observation of the outburst.

Another possibility is that the frequency second derivative we measured (or at least a significant fraction of it) is linked to the magnetospheric activity of SGR 1833−0832. In the magnetar scenario the spin derivative is in fact expected to increase while the magnetospheric twist is growing, i.e. for instance in periods preceding large outbursts, and to decrease in the aftermath (see e.g. Thompson et al. 2002; Beloborodov 2009). On the other hand, as pointed out by Beloborodov (2009), a negative $\ddot{\nu}$ following a period of bursting activity (as that detected here) can be still accounted for if a magnetospheric twist is suddenly implanted, but its strength is moderate (twist angle less than $\sim$1 rad). Then the twist may still grow for a while in spite of the luminosity released by dissipation monotonically decreases. Only after the twist angle has reached its maximum value, it will start to decay, together with the torque.

Nevertheless, the timing properties of the source appear consistent with those typically observed in the AXP/SGR class. The spectral characteristics of SGR 1833−0832 are instead somewhat less usual. The X-ray spectrum is well described by a single blackbody with temperature $kT \sim 1.2$ keV, definitely higher than what generally is observed both in transient and 'persistent' magnetars ($kT \lesssim 0.7$ keV, with the exception of SGR 0418+5729; Esposito et al. 2010b; Rea et al. 2010). We cannot however exclude that the high temperature of SGR 1833−0832 partially results from a bias in the spectral fits that, given the paucity of counts below $\sim$2–3 keV (owing to the large absorption), acts in the direction of increasing temperature, in order to account for a second spectral component which cannot be properly modelled (see Section 3.2).

The large increase in flux, a factor $\gtrsim$20 above the quiescent level, is indicative of a rather powerful event, not dissimilar from those observed in other transient sources. This, however, seems to be in contrast with the low level of activity seen in SGR 1833−0832, from which only few bursts were detected (Göğüş et al. 2010a). A scenario in which we are presently witnessing the later stages of an outburst which was caught during its decay rather than at its onset, could account for the low activity but seems difficult to reconcile with the current high value of the temperature (if the

[10] The indicator commonly used to quantify the amount of timing noise in radio pulsars is the Δ_8 parameter introduced by Arzoumanian et al. (1994). The value computed with the ephemeris of SGR 1833−0832 given in Table 3 is $\Delta_8 \simeq 4.2$, which is much higher than the typical values measured for radio pulsars (roughly between 0 and −5; Arzoumanian et al. 1994; Hobbs, Lyne & Kramer 2010). Moreover, considering the correlation between timing noise and spin-down rate, one would expect for SGR 1833−0832 Δ_8 to be approximately −0.6 (Hobbs et al. 2010).

Downloaded from http://mnras.oxfordjournals.org/ at University College London on April 29, 2013

thermal component in the spectrum of SGR 1833−0832 is indeed at $kT \sim 1.2$ keV). A further possibility might be that SGR 1833−0832 experienced a (crustal) heating episode which, however, was not accompanied by (or did not trigger) a twisting of the external field, as possibly suggested by the non-detection of a hard X-ray tail. In this case, however, an alternative explanation, not related to the twist evolution, for the presence of a negative $\ddot{\nu}$ must be sought (perhaps a long-term postglitch recovery, see above).

Immediately after the BAT trigger that led to the discovery of SGR 1833−0832, its observed flux was of $\sim 3.8 \times 10^{-12}$ erg cm^{-2} s^{-1}, and it decreased by ≈75 per cent during the following 5 months (which is not unusual for magnetars; e.g. Rea & Esposito 2011), to $\sim 1.1 \times 10^{-12}$ erg cm^{-2} s^{-1}. Although present data do not allow us to discriminate among different decay patterns, the flux evolution can be satisfactorily described by a broken power law, similar to the case of SGR 0418+5729. The flux of SGR 1833−0832 remained fairly constant for about 20 d ($\alpha_1 \sim 0$), when the decay index changed to $\alpha_2 \sim -0.5$. Interestingly, also the decay of SGR 0418+5729 exhibited a break at ∼20 d (Esposito et al. 2010b). As in the case of SGR 0418+5729 (see the discussion in Esposito et al. 2010b), the presence of a break, together with the rather flat decay indices, might be difficult to reconcile with the predictions of the deep crustal heating scenario (Lyubarsky, Eichler & Thompson 2002), $F \propto t^{-n/3}$ with $n \sim 2$–3. This model provides a satisfactory description of the flux decay in SGR 1627-41 (Kouveliotou et al. 2003, although subsequent analyses found no evidence for the plateau around ∼400–800 d predicted by the model; Mereghetti et al. 2006) and AXP 1E 2259+586 (Zhu et al. 2008). At the same time, however, it cannot explain the variety of decay patterns which emerged from recent observations of SGRs/AXPs (e.g. Rea et al. 2009). This may reflect the intrinsic limitations of the model (which relies on a simplified, one-dimensional treatment), or point towards the existence of different heating mechanisms which are at work during the outbursts of magnetars, like in the case of SGR 1833−0832.

Prompted by previous detections of a transient (pulsed) radio emission following X-ray transient activity in other magnetars (Camilo et al. 2006, 2007; Burgay et al. 2009), we observed SGR 1833−0832 with the Australia Telescope Compact Array (ATCA) and the 64-m Parkes Radio Telescope (Burgay et al. 2010; Wieringa et al. 2010). No evidence for radio emission was found, down to flux densities of 0.9 and 0.09 mJy for the continuum and pulsed emissions, respectively. Similar upper limits on the pulsed radio emission, 0.1 mJy at 1.38 GHz and 0.2 mJy at 2.28 GHz for a 10 per cent duty cycle, were obtained with the Westerbork Radio Synthesis Telescope in the same days (but not simultaneously with our observations; Göğüş et al. 2010a). Despite this rather intensive coverage, the negative results of radio searches performed so far on SGR 1833−0832 cannot anyway be taken as conclusive because of the rapid variability of the pulsed flux shown by the known radio magnetars (see e.g. Burgay et al. 2009). Moreover, for a distance $d = 10$ kpc these limits translates into a pseudo-luminosity $L = Sd^2 \approx 10$ mJy kpc^2, which is significantly smaller than the 1.4-GHz luminosity of the other known radio magnetars at their peak (∼100–400 mJy kpc^2; Camilo et al. 2006, 2007; Levin et al. 2010) but still much larger than the luminosities of some known ordinary radio pulsars.[11]

[11] See the online version of the Australia Telescope National Facility (ATNF) pulsar catalogue (Manchester et al. 2005) at http://www.atnf.csiro.au/research/pulsar/psrcat/.

6.2 PSR B1830–08 and HESS J1834–08

The discovery of the X-ray PWN generated by PSR B1830−08, suggestive of a pulsar bow-shock and a possible diffuse emission trailing the pulsar proper motion, provides new elements to the identification of HESS J1834−087. Accounting for a systematic 20 per cent uncertainty, the distance of PSR B1830−08 is compatible with the one of W41, 4.0 ± 0.2 kpc (Tian et al. 2007), which is likely associated to HESS J1834−087 given the low probability of a chance superposition. The pulsar spin-down age is also consistent with the dynamical age of remnant, roughly 100 kyr (Tian et al. 2007). As pointed out by Mukherjee et al. (2009), the pulsar moves fast enough to have reached its current position starting only 40 kyr from the geometric centre of the remnant (see also Fig. 6, left-hand panel).

However, the Gamma-ray to X-ray flux ratio, $F_{(\mathrm{E}>1\,\mathrm{TeV})}/F_{(2-10\,\mathrm{keV})} \sim 50$ for the compact emission and ∼10 for the total X-ray emission, is lower than the one expected from the inverse correlation between this quantity and $\dot{E}$ (Mattana et al. 2009), which should be around 600 for PSR B1830−08. If HESS J1834−08 is the relic PWN generated by PSR B1830−08, it is not very efficient in radiating in TeV gamma rays. Otherwise, it may be unrelated to PSR B1830−08. The non-detection of a more extended X-ray emission trailing the pulsar does not support the association with HESS J1834−087 either. Higher resolution and longer X-ray observations are needed to establish the nature of the halo and the detailed morphology of the compact emission, as well as singling out a possible contribution from the pulsar magnetosphere to the compact emission.

ACKNOWLEDGMENTS

We thank the referee, Vicky Kaspi, for valuable and constructive comments. This research is based on observations obtained with *XMM–Newton*, an ESA science mission with instruments and contributions directly funded by ESA Member States and NASA. We thank Norbert Schartel and the staff of the *XMM–Newton* Science Operation Center for promptly scheduling and executing our observations. The *RXTE* and *Swift* data were obtained through the HEASARC Online Service, provided by the NASA/GSFC. We thank the *Swift* PI, Neil Gehrels, the *Swift* duty scientists and science planners for making our *Swift* target of opportunity observations possible. We thank Hans Krimm for re-analysing the *Swift*/BAT transient monitor and survey data for the time period following the outburst. We thank Philip Edwards of CSIRO for prompt allocations of observing time at the Parkes Observatory and the ATCA. The Parkes Observatory and the ATCA are part of the Australia Telescope, which is funded by the Commonwealth of Australia for operation as a National Facility managed by CSIRO. The Italian authors acknowledge the partial support from ASI (ASI/INAF contracts I/009/10/0, I/011/07/0, I/010/06/0, I/088/06/0 and AAE TH-058). PE acknowledges financial support from the Autonomous Region of Sardinia through a research grant under the programme PO Sardegna FSE 2007-2013, L.R. 7/2007 'Promoting scientific research and innovation technology in Sardinia'. FM and DG acknowledge the CNES for financial funding. NR is supported by a Ramón y Cajal fellowship.

REFERENCES

Aharonian F. et al., 2006, ApJ, 636, 777
Albert J. et al., 2006, ApJ, 643, L53

Downloaded from http://mnras.oxfordjournals.org/ at University College London on April 29, 2013

Anders E., Grevesse N., 1989, Geochim. Cosmochim. Acta, 53, 197
Arnaud K. A., 1996, in Jacoby G. H., Barnes J., eds, ASP Conf. Ser. Vol. 101, Astronomical Data Analysis Software and Systems V. Astron. Soc. Pac., San Francisco, p. 17
Arzoumanian Z., Nice D. J., Taylor J. H., Thorsett S. E., 1994, ApJ, 422, 671
Balucinska-Church M., McCammon D., 1992, ApJ, 400, 699
Barthelmy S. D. et al., 2010, GCN Circ., 10528
Bartko H., Bednarek W., 2008, MNRAS, 385, 1105
Beloborodov A. M., 2009, ApJ, 703, 1044
Bernardini F. et al., 2009, A&A, 498, 195
Bernardini F. et al., 2011, A&A, 529, A19
Bucciantini N., Amato E., Del Zanna L., 2005, A&A, 434, 189
Burgay M., Israel G. L., Possenti A., Rea N., Esposito P., Mereghetti S., Tiengo A., Götz D., 2009, Astron. Telegram, 1913
Burgay M. et al., 2010, Astron. Telegram, 2515
Burrows D. N. et al., 2005, Space Sci. Rev., 120, 165
Camilo F., Ransom S. M., Halpern J. P., Reynolds J., Helfand D. J., Zimmerman N., Sarkissian J., 2006, Nat, 442, 892
Camilo F., Ransom S. M., Halpern J. P., Reynolds J., 2007, ApJ, 666, L93
Cordes J. M., Lazio T. J. W., 2002, preprint (astro-ph/0207156)
Dall'Osso S., Israel G. L., Stella L., Possenti A., Perozzi E., 2003, ApJ, 599, 485
De Luca A., Molendi S., 2004, A&A, 419, 837
Dib R., Kaspi V. M., Gavriil F. P., 2008, ApJ, 673, 1044
Dickey J. M., Lockman F. J., 1990, ARA&A, 28, 215
Duncan R. C., Thompson C., 1992, ApJ, 392, L9
Enoto T. et al., 2009, ApJ, 693, L122
Esposito P. et al., 2008, MNRAS, 390, L34
Esposito P. et al., 2009, ApJ, 690, L105
Esposito P., Israel G. L., Stella L., Rea N., Tiengo A., 2010a, Astron. Telegram, 2494
Esposito P. et al., 2010b, MNRAS, 405, 1787
Esposito P. et al., 2010c, Astron. Telegram, 2550
Gaensler B. M., Johnston S., 1995, MNRAS, 275, L73
Gaensler B. M., Slane P. O., 2006, ARA&A, 44, 17
Gaensler B. M., van der Swaluw E., Camilo F., Kaspi V. M., Baganoff F. K., Yusef-Zadeh F., Manchester R. N., 2004, ApJ, 616, 383
Gelbord J. M., Vetere L., 2010, GCN Circ., 10531
Gelbord J. M. et al., 2010, GCN Circ., 10526
Ghizzardi S., 2001, in Flight Calibration of the PSF for the PN Camera, Calibration document XMM-SOC-CAL-TN-0022. ESA, Madrid, http://xmm.vilspa.esa.es/docs/documents/CAL-TN-0022-1-0.ps.gz
Gotthelf E. V., Halpern J. P., Buxton M., Bailyn C., 2004, ApJ, 605, 368
Göğüş E. et al., 2010a, ApJ, 718, 331
Göğüş E., Strohmayer T., Kouveliotou C., Woods P., 2010b, Astron. Telegram, 2493
Hill J. E. et al., 2004, in Flanagan K. A., Siegmund O. H. W., eds, Proc. SPIE Conf. Ser. Vol. 5165, X-ray and Gamma-ray Instrumentation for Astronomy XIII. SPIE, Bellingham, p. 217
Hobbs G., Lyne A. G., Kramer M., Martin C. E., Jordan C., 2004, MNRAS, 353, 1311
Hobbs G., Lyne A. G., Kramer M., 2010, MNRAS, 402, 1027
Ibrahim A. I. et al., 2004, ApJ, 609, L21
Israel G. L., Campana S., Dall'Osso S., Muno M. P., Cummings J., Perna R., Stella L., 2007a, ApJ, 664, 448
Israel G. L., Götz D., Zane S., Dall'Osso S., Rea N., Stella L., 2007b, A&A, 476, L9
Jahoda K., Swank J. H., Giles A. B., Stark M. J., Strohmayer T., Zhang W., Morgan E. H., 1996, in Siegmund O. H. W., Gummin M. A., eds, Proc. SPIE Conf. Ser. Vol. 2808, EUV, X-Ray, and Gamma-Ray Instrumentation for Astronomy VII. SPIE, Bellingham, p. 59
James F., Roos M., 1975, Comput. Phys. Commun., 10, 343
Kargaltsev O., Pavlov G. G., 2008, in Bassa C., Wang Z., Cumming A., Kaspi V. M., eds, AIP Conf. Proc. Vol. 983, 40 Years of Pulsars: Millisecond Pulsars, Magnetars and More. Am. Inst. Phys., New York, p. 171
Kassim N. E., 1992, AJ, 103, 943
Kouveliotou C. et al., 2003, ApJ, 596, L79
Lamb R. C., Fox D. W., Macomb D. J., Prince T. A., 2002, ApJ, 574, L29
Levin L. et al., 2010, ApJ, 721, L33
Lorimer D. R., Kramer M., 2004, Handbook of Pulsar Astronomy. Cambridge Univ. Press, Cambridge
Lyubarsky Y., Eichler D., Thompson C., 2002, ApJ, 580, L69
Manchester R. N., Hobbs G. B., Teoh A., Hobbs M., 2005, AJ, 129, 1993
Mattana F. et al., 2009, ApJ, 694, 12
Mereghetti S., 2008, A&AR, 15, 225
Mereghetti S. et al., 2005, ApJ, 628, 938
Mereghetti S. et al., 2006, A&A, 450, 759
Misanovic Z., Kargaltsev O., Pavlov G., 2011, preprint (arXiv:1101.1342)
Mukherjee R., Gotthelf E. V., Halpern J. P., 2009, ApJ, 691, 1707
Overbeck J. W., 1965, ApJ, 141, 864
Paczynski B., 1992, Acta Astron., 42, 145
Palmer D., Gelbord J. M., 2010, GCN Circ., 10537
Possenti A., Cerutti R., Colpi M., Mereghetti S., 2002, A&A, 387, 993
Rea N., Esposito P., 2011, in Torres D. F., Rea N., eds, Astrophysics and Space Science Proceedings, High-Energy Emission from Pulsars and their Systems. Springer, Berlin, p. 247
Rea N. et al., 2009, MNRAS, 396, 2419
Rea N. et al., 2010, Sci, 330, 944
Rivera Ingraham A., van Kerkwijk M. H., 2010, ApJ, 710, 797
Staveley-Smith L. et al., 1996, Publ. Astron. Soc. Australia, 13, 243
Strüder L. et al., 2001, A&A, 365, L18
Tam C. R., Kaspi V. M., Gaensler B. M., Gotthelf E. V., 2006, ApJ, 652, 548
Taylor J. H., Manchester R. N., Lyne A. G., 1993, ApJS, 88, 529
Thompson C., Duncan R. C., 1995, MNRAS, 275, 255
Thompson C., Duncan R. C., 1996, ApJ, 473, 322
Thompson C., Lyutikov M., Kulkarni S. R., 2002, ApJ, 574, 332
Tian W. W., Li Z., Leahy D. A., Wang Q. D., 2007, ApJ, 657, L25
Tiengo A. et al., 2010, ApJ, 710, 227
Torii K., Kinugasa K., Katayama K., Tsunemi H., Yamauchi S., 1998, ApJ, 503, 843
Turner M. J. L. et al., 2001, A&A, 365, L27
Vasisht G., Gotthelf E. V., Torii K., Gaensler B. M., 2000, ApJ, 542, L49
Wieringa M. H. et al., 2010, Astron. Telegram, 2521
Woods P. M., Thompson C., 2006, in Levin W. H. G., van der Klis M., eds, Compact Stellar X-ray Sources. Cambridge Univ. Press, Cambridge, p. 547
Zhu W., Kaspi V. M., Dib R., Woods P. M., Gavriil F. P., Archibald A. M., 2008, ApJ, 686, 520

This paper has been typeset from a TEX/LATEX file prepared by the author.

Downloaded from http://mnras.oxfordjournals.org/ at University College London on April 29, 2013